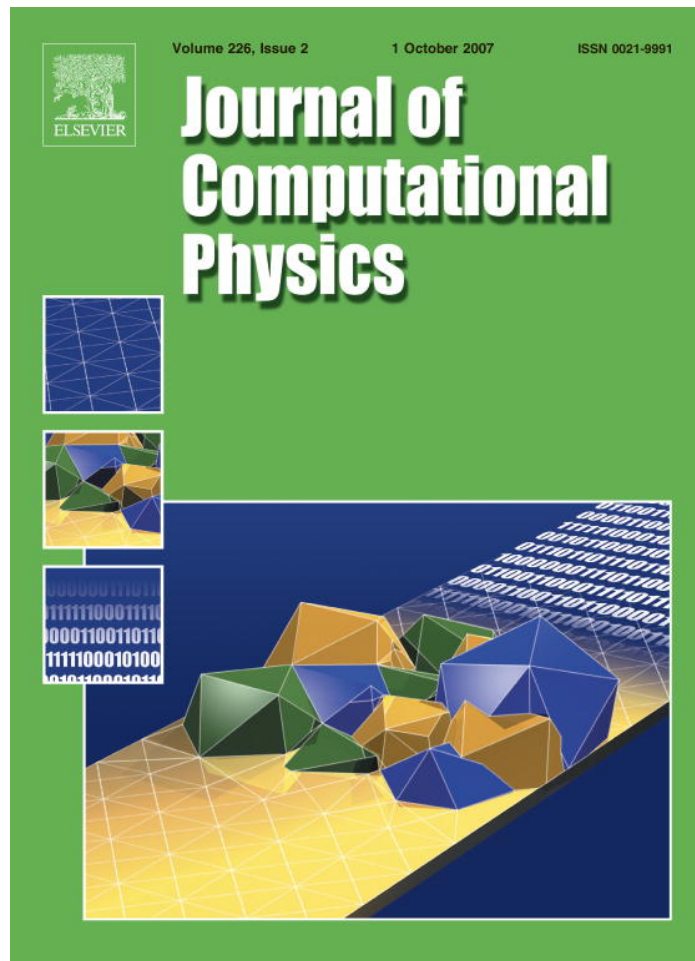


Provided for non-commercial research and education use.  
Not for reproduction, distribution or commercial use.



This article was published in an Elsevier journal. The attached copy is furnished to the author for non-commercial research and education use, including for instruction at the author's institution, sharing with colleagues and providing to institution administration.

Other uses, including reproduction and distribution, or selling or licensing copies, or posting to personal, institutional or third party websites are prohibited.

In most cases authors are permitted to post their version of the article (e.g. in Word or Tex form) to their personal website or institutional repository. Authors requiring further information regarding Elsevier's archiving and manuscript policies are encouraged to visit:

<http://www.elsevier.com/copyright>



# Electronic structure calculations in a uniform magnetic field using periodic supercells

Eunseok Lee <sup>a,\*</sup>, Wei Cai <sup>a</sup>, Giulia A. Galli <sup>b</sup>

<sup>a</sup> Department of Mechanical Engineering, Stanford University, CA 94305-4040, USA

<sup>b</sup> Department of Chemistry, University of California, Davis, CA 95616, USA

Received 20 October 2006; received in revised form 5 April 2007; accepted 16 May 2007

Available online 8 June 2007

---

## Abstract

We have recently presented a method that allows one to use periodic supercells in *ab initio* electronic structure calculations in the presence of a finite magnetic field [Phys. Rev. Lett. 92 (2004) 186402]. This method retains the simplicity and efficiency of plane-wave basis sets and Fourier transforms. The original formulation was developed for cubic cell and for the  $\mathbf{k} = (0, 0, 0)$  point of the supercell Brillouin zone, and here we extend the formalism to arbitrarily tilted supercells and to the case of non-zero  $\mathbf{k}$ -points. Implementation details are discussed, together with numerical benchmarks. Finally, first principles calculations of magnetic band structures are presented.

© 2007 Elsevier Inc. All rights reserved.

PACS: 71.15.-m; 71.10.-w; 71.70.Di

Keywords: Electronic structure calculation; Magnetic band structure; Magnetic periodic boundary condition; Tilted supercell

---

## 1. Introduction

In the last two decades, *ab initio* electronic structure methods based on density functional theory (DFT) have been widely used to investigate the structural and electronic properties of molecules, clusters, and bulk condensed matter [1]. In particular, the formulation of *ab initio* molecular dynamics (MD) [2] has permitted key progress in the prediction of finite temperature properties of materials entirely from first principles. The most widely used implementation of *ab initio* MD and of electronic structure calculations for condensed systems is based on pseudopotentials and plane-wave (PW) basis sets. The use of PW has several advantages. The convergence of total energy and force calculations can be controlled by a single parameter (kinetic energy cut-off) and improved to arbitrary accuracy. Atomic forces can be easily computed without evaluating the so-called Pulay contributions [3] and efficient fast Fourier transform (FFT) techniques can be applied. PW basis sets call for the use of periodic boundary conditions (PBC), which

---

\* Corresponding author.

E-mail address: [euniv@stanford.edu](mailto:euniv@stanford.edu) (E. Lee).

conveniently eliminate surface and interface effects and allow for a small simulation cell to mimic the bulk behavior of materials.

To date, most *ab initio* investigations have focused on ground state properties in the absence of external electromagnetic fields. Due to technical difficulties in describing finite fields within PW formulations and using PBC, almost all studies with electromagnetic fields have been carried out perturbatively. Within this approach, simulations are performed at zero field and electric polarizability and magnetic susceptibility are computed based on linear response theory [4]. This technique can be used only when the applied field is sufficiently small, and there are many situations, e.g. condensed systems – notably hydrogen – in stars and planets [5], where the effect of a finite field cannot be treated in a perturbative fashion.

Recently, there has been progress in explicitly incorporating a finite electric field in condensed-phase *ab initio* simulations [6], and a non-perturbative Bloch solution of the Schrödinger's equation in a finite magnetic field was proposed [7]. In addition, we have proposed a formulation of self-consistent *ab initio* calculations within DFT where the effect of a finite, uniform magnetic field is treated in a non-perturbative manner, using algorithms based on PW basis sets and FFT [8]. These algorithms have been key in the development of simple and efficient first principles MD techniques. While the applicability of the proposed method has been demonstrated on several problems, including one and two electrons in a quantum well (treated by using configuration interaction), a hydrogen molecule (at the Hartree–Fock level), and a dense deuterium fluid (at the DFT level), the original method was only developed for cubic supercells and the case of zero  $\mathbf{k}$ -point ( $\Gamma$ -point). However, in many applications, it may be more convenient to use a non-orthogonal supercell, e.g. to model crystals with a non-cubic primitive cell. The orientation of the magnetic field can also be changed conveniently if one can simply tilt the repeat vector of the supercell. At the same time, computing the electronic band structure under magnetic field requires a method that can be applied to the case of non-zero  $\mathbf{k}$ -points. Non-zero  $\mathbf{k}$ -point calculations are also important to study electron transport problems.

In this paper, we extend the method presented in Ref. [8] to arbitrarily tilted supercells and the case of non-zero  $\mathbf{k}$ -points. Section 2 formulates the problem of the incompatibility between periodic boundary conditions and the presence of a uniform magnetic field, and it introduces magnetic periodic boundary conditions (MPBC) as a solution. Section 3 explains the implementation details of MPBC in cubic supercells with the  $\Gamma$ -point ( $\mathbf{k} = (0, 0, 0)$ ). In Section 4, the method is generalized to tilted supercells and non-zero  $\mathbf{k}$ -points. Benchmark results on the computational cost and numerical accuracy of the method are presented in Section 5.

## 2. Problem statement

### 2.1. Boundary conditions for electron wave functions

Among existing *ab initio* methods to simulate condensed matter systems, one of the most popular and successful ones is based on density functional theory (DFT), with single particle orbitals expanded in plane waves and makes use of supercells and periodic boundary conditions (PBC). The Hamiltonian of a system containing a single electron (considered here for simplicity), in the absence of an external electric or magnetic field, is given by:

$$\hat{H} = \frac{|\mathbf{p}|^2}{2m} + V(\mathbf{x}), \quad (1)$$

where  $\mathbf{p} = -i\hbar\nabla$  is the momentum operator and  $V(\mathbf{x})$  is the potential energy function describing the electron–nuclei interaction.

If  $V(\mathbf{x})$  is periodic in space, i.e.,

$$V(\mathbf{x} + \mathbf{c}_i) = V(\mathbf{x}), \quad (2)$$

where  $\mathbf{c}_i$ ,  $i = 1, 2, 3$ , are three repeat vectors of a *supercell*, then, according to Bloch's theorem, an eigen-function of the Hamiltonian satisfies the following boundary condition:

$$\psi(\mathbf{x} - \mathbf{c}_i) = \exp[-i\boldsymbol{\kappa} \cdot \mathbf{c}_i]\psi(\mathbf{x}) \quad (3)$$

for arbitrary  $\boldsymbol{\kappa}$ . Using a standard notation for a Bloch wave function  $u(\mathbf{x})$ , we have

$$\psi(\mathbf{x}) = u(\mathbf{x})e^{i\mathbf{k}\cdot\mathbf{x}} \quad (4)$$

with  $u(\mathbf{x})$  satisfying periodic boundary conditions (PBC),

$$u(\mathbf{x} - \mathbf{c}_i) = u(\mathbf{x}). \quad (5)$$

There are several advantages in using PBC. First, PBC conveniently eliminate artificial surface effects and are thus an ideal choice to model bulk material properties. Second, if an electron wave function satisfies PBC, then it can be expanded as a linear superposition of plane waves. The (Fourier) coefficients of this expansion constitute a natural discretization of the wave function. The convergence of this numerical representation can be conveniently controlled by a single parameter, the maximum kinetic energy adopted in the plane wave expansion. Third, when expanding a wave function  $\psi$  in plane waves, one can evaluate  $\hat{H}\psi$  by using highly efficient fast Fourier transform (FFT) algorithms.

However, in principle this method cannot be generalized in a straightforward manner to include the presence of an external electric field  $\mathbf{E}$  and magnetic field  $\mathbf{B}$ .  $\mathbf{B}$  and  $\mathbf{E}$  do not enter the Hamiltonian  $\hat{H}$  of the system, but their potential fields do:

$$\hat{H} = \frac{|\mathbf{p} + e\mathbf{A}(\mathbf{x})|^2}{2m} + V(\mathbf{x}) - e\phi(\mathbf{x}), \quad (6)$$

where  $\mathbf{A}$  is the vector potential of the magnetic field  $\mathbf{B}$  and  $\phi(\mathbf{x})$  is the scalar potential of the electric field  $\mathbf{E}$ ,

$$\mathbf{E} = -\nabla\phi(\mathbf{x}), \quad (7)$$

$$\mathbf{B} = \nabla \times \mathbf{A}(\mathbf{x}). \quad (8)$$

For uniform electric or magnetic fields, the potential fields  $\phi$  or  $\mathbf{A}$  are linear functions of  $\mathbf{x}$ . As a result, the Hamiltonian is no longer a periodic function of  $\mathbf{x}$ , even though the nuclear potential  $V(\mathbf{x})$  is periodic. Consequently, PBC can no longer be applied to electronic wave functions, which makes it difficult to use a plane wave basis and FFT techniques.

In the following we discuss how to incorporate a finite and uniform magnetic field into *ab initio* simulations and retain the conceptual simplicity of PW expansions.

## 2.2. Translational invariance under magnetic field

For an electron moving in a uniform magnetic field, the Lorentz force does zero work because it is always perpendicular to the electron velocity. Consequently, we cannot distinguish two points in space under a uniform magnetic field by measuring the energy of the electron. In classical mechanics, an isolated electron orbits in a circle with specific radius and frequency in a uniform magnetic field. If we were to transport the electron to a different location in space, it will again orbit with the same radius and frequency. This intuitively suggests that the physical space in which the electron moves is still translationally invariant even in the presence of a magnetic field [9]. Thus a “periodic” boundary condition may still be applied to an electron in a uniform magnetic field.

In quantum mechanics, the translational invariance of space is apparently broken by the vector potential, which is a linear function of space. However, we can use *gauge invariance* to restore translational invariance. Multiple vector potentials  $\mathbf{A}(\mathbf{x})$  can give rise to the same magnetic field through  $\mathbf{B} = \nabla \times \mathbf{A}(\mathbf{x})$ . We can add to  $\mathbf{A}$  the gradient of an arbitrary scalar field,

$$\mathbf{A}'(\mathbf{x}) = \mathbf{A}(\mathbf{x}) - \nabla\lambda(\mathbf{x}) \quad (9)$$

without changing the magnetic field, i.e.,

$$\mathbf{B} = \nabla \times \mathbf{A}(\mathbf{x}) = \nabla \times \mathbf{A}'(\mathbf{x}). \quad (10)$$

When a gauge transformation is applied to the vector potential, Eq. (9), the eigen-function  $\psi'(\mathbf{x})$  of the new Hamiltonian  $\hat{H}'$  can be obtained from the eigen-function  $\psi(\mathbf{x})$  of the old Hamiltonian  $\hat{H}$  by multiplying by a phase factor,

$$\psi'(\mathbf{x}) = \exp\left[i\frac{e}{\hbar}\lambda(\mathbf{x})\right]\psi(\mathbf{x}). \quad (11)$$

Specifically, when  $\lambda(\mathbf{x}) = \mathbf{n} \cdot \mathbf{x}$ , then the gauge transformation corresponds to adding an arbitrary constant vector to the vector potential, and the eigen-function is multiplied by a plane wave,

$$\mathbf{A}'(\mathbf{x}) = \mathbf{A}(\mathbf{x}) - \mathbf{n}, \quad (12)$$

$$\psi'(\mathbf{x}) = \exp \left[ i \frac{e}{\hbar} \mathbf{n} \cdot \mathbf{x} \right] \psi(\mathbf{x}). \quad (13)$$

Because the absolute phase of a wave function is not an observable, the change of wave function phase upon a gauge transformation can be regarded as a theoretical artifact. On the other hand, the electron density,  $\rho(\mathbf{x}) = |\psi(\mathbf{x})|^2$ , which can be measured experimentally, remains unchanged when applying a gauge transformation.

### 2.3. Magnetic periodic boundary condition

The gauge transformation expressed by Eqs. (12) and (13) has been used by Brown [10] to design magnetic periodic boundary conditions (MPBC) for electron wave functions under a uniform magnetic field. The Hamiltonian of an electron under a uniform magnetic field is

$$\hat{H} = \frac{|\mathbf{p} + e\mathbf{A}(\mathbf{x})|^2}{2m} + V(\mathbf{x}). \quad (14)$$

For  $V(\mathbf{x})$  periodic in space, as in Eq. (2), the eigen-function of the Hamiltonian can be made to satisfy MPBC,

$$\psi(\mathbf{x} - \mathbf{c}_i) = \exp \left[ i \frac{e}{\hbar} \mathbf{A}(\mathbf{c}_i) \cdot \mathbf{x} - i\boldsymbol{\kappa} \cdot \mathbf{c}_i \right] \psi(\mathbf{x}) \quad (15)$$

for arbitrary  $\boldsymbol{\kappa}$ . If we define a Bloch wave function  $u(\mathbf{x})$  through Eq. (4), then  $u(\mathbf{x})$  satisfies the following boundary condition:

$$u(\mathbf{x} - \mathbf{c}_i) = \exp \left[ i \frac{e}{\hbar} \mathbf{A}(\mathbf{c}_i) \cdot \mathbf{x} \right] u(\mathbf{x}). \quad (16)$$

When the magnetic field is zero,  $\mathbf{A}(\mathbf{x}) = 0$ , MPBC for  $\psi(\mathbf{x})$  reduces to the Bloch condition,

$$\psi(\mathbf{x} - \mathbf{c}_i) = \exp[-i\boldsymbol{\kappa} \cdot \mathbf{c}_i] \psi(\mathbf{x}) \quad (17)$$

and MPBC for  $u(\mathbf{x})$  reduces to:

$$u(\mathbf{x} - \mathbf{c}_i) = u(\mathbf{x}). \quad (18)$$

If  $\psi(\mathbf{x})$  satisfies MPBC, then the electron density  $\rho(\mathbf{x}) = |\psi(\mathbf{x})|^2$  always satisfies PBC, even when the magnetic field is non-zero.

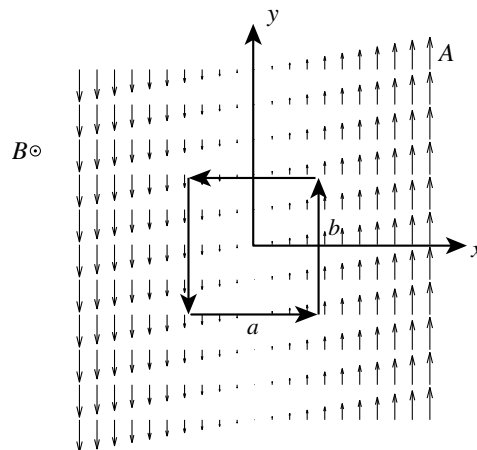


Fig. 1. MPBC in the Landau gauge. The magnetic field is along  $z$  (out of plane),  $\mathbf{B} = B\mathbf{e}_z$  and the vector potential is along  $y$ ,  $\mathbf{A} = Bx\mathbf{e}_y$ . The supercell is an  $a \times b$  rectangle.

As a specific example, consider a cubic supercell, whose three repeat vectors are  $\mathbf{c}_1 = a\mathbf{e}_x$ ,  $\mathbf{c}_2 = b\mathbf{e}_y$ ,  $\mathbf{c}_3 = c\mathbf{e}_z$ , where  $\mathbf{e}_x$ ,  $\mathbf{e}_y$  and  $\mathbf{e}_z$  are unit vectors along  $x$ ,  $y$ ,  $z$  axes, respectively. Let the magnetic field be along the  $z$  axis, i.e.  $\mathbf{B} = B\mathbf{e}_z$ , and choose the Landau gauge,  $\mathbf{A} = Bx\mathbf{e}_y$ , as shown in Fig. 1. In this case, MPBC (Eq. (16)) can be expressed as

$$u(x - a, y, z) = \exp\left[i\frac{eBa}{\hbar}y\right]u(x, y, z), \quad (19)$$

$$u(x, y - b, z) = u(x, y, z), \quad (20)$$

$$u(x, y, z - c) = u(x, y, z). \quad (21)$$

The boundary condition in  $x$  direction is coupled with  $y$ , as in Eq. (19). On the other hand, the boundary condition in  $z$  direction is simply periodic, as in Eq. (21), and independent of  $x$  and  $y$ . For simplicity, in the following we will ignore the  $z$  dependence of the wave function and discuss a two-dimensional wave function  $u(x, y)$ .

### 3. MPBC in orthogonal supercell with $\kappa = 0$

#### 3.1. Plane-wave-basis *ab initio* algorithm at $\mathbf{B} = 0$

The main purpose of this section is to describe how to implement MPBC in an *ab initio* simulation. To this end, we first summarize the basic computational strategy of *ab initio* simulations in the absence of a magnetic field. In this case, the wave function  $u(x, y)$  satisfies PBC and can be expressed as a sum of plane waves,

$$u(x, y) = \sum_{k_x, k_y} c(k_x, k_y) \exp(ik_x x + ik_y y), \quad (22)$$

where  $k_x = mG_x$ ,  $k_y = nG_y$ ,  $G_x = 2\pi/a$ ,  $G_y = 2\pi/b$ , and  $m$  and  $n$  are integers. In practice, a truncation is applied, so that only a finite number of plane waves is included in the sum. The Fourier transform of Eq. (22) is:

$$c(k_x, k_y) = \frac{1}{ab} \int_{-a/2}^{a/2} \int_{-b/2}^{b/2} u(x, y) \exp(-ik_x x - ik_y y) dx dy, \quad (23)$$

$u(x, y)$  and  $c(k_x, k_y)$  are the real-space and reciprocal-space representations of the electronic wave function. One can efficiently go from real to Fourier space by using fast Fourier transform (FFT) algorithms. For simplicity, consider the case of  $\kappa = 0$  (Eq. (4)), so that  $u$  satisfies the same equation as  $\psi$ ,

$$\hat{H}u(x, y) = Eu(x, y). \quad (24)$$

The key step involved in solving Eq. (24) is the evaluation of  $\hat{H}u(x, y)$  for an arbitrary *trial* function  $u(x, y)$ . Eq. (24) can then be solved iteratively, e.g. using the steepest descent or the conjugate gradient algorithm [11], with  $\hat{H}u(x, y)$  as the gradient vector. Alternatively,  $\hat{H}u(x, y)$  can be used for Car–Parrinello molecular dynamics (CPMD) simulations [2].

In the absence of a magnetic field, the Hamiltonian can be separated into the kinetic energy operator  $\hat{T}$  and potential energy operator  $\hat{V}$ , which are best evaluated in reciprocal space and real space, respectively. The evaluation of the potential energy operator is simply a multiplication in real space,

$$\hat{V}u(x, y) = V(x, y)u(x, y). \quad (25)$$

The evaluation of the kinetic energy operator is simply a multiplication in reciprocal space,

$$\hat{T}c(k_x, k_y) = \frac{\hbar^2(k_x^2 + k_y^2)}{2m}c(k_x, k_y). \quad (26)$$

Therefore, the two parts of  $\hat{H}u(x, y)$  can be evaluated separately in the two spaces and then assembled together by FFT, as illustrated in Fig. 2.

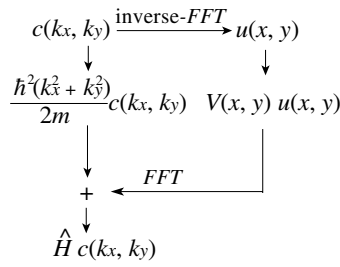


Fig. 2. Flow chart for computing  $\hat{H}c(k_x, k_y)$  given an arbitrary trial wave function  $c(k_x, k_y)$  (represented in reciprocal space). The kinetic energy operator  $\hat{T}$  is a multiplication,  $\frac{\hbar^2(k_x^2 + k_y^2)}{2m}c(k_x, k_y)$ , in reciprocal space. The potential energy operator  $\hat{V}$  is a multiplication,  $V(x, y)u(x, y)$ , in real space. The two parts are assembled together by fast Fourier transform (FFT).

Numerically, the transformation between  $u(x, y)$  and  $c(k_x, k_y)$  can be done in one step by a two-dimensional FFT. However, to set the stage for the  $B \neq 0$  case, let us consider a two-step process. As shown in Fig. 3,  $u(x, y)$  is first Fourier transformed along  $y$ -axis, leading to  $f(x, k_y)$ , which is then Fourier transformed along  $x$ -axis, leading to  $c(k_x, k_y)$ .  $f(x, k_y)$  is the representation of the wave function in a so-called *intermediate* space, since  $k_y$  is a reciprocal-space variable and  $x$  is a real-space variable. In real space,  $u(x, y)$  is a periodic function of two continuous variables,  $-a/2 \leq x \leq a/2$  and  $-b/2 \leq y \leq b/2$ ,

$$u(x - a, y) = u(x, y), \tag{27}$$

$$u(x, y - b) = u(x, y). \tag{28}$$

The intermediate space wave function,  $f(x, k_y)$ , is a function of a continuous variable,  $-a/2 \leq x \leq a/2$ , and a discrete variable,  $k_y = nG_y$ . For each  $k_y$ ,  $f(x, k_y)$  is a periodic function of  $x$ ,

$$f(x - a, k_y) = f(x, k_y). \tag{29}$$

Therefore,  $f(x, k_y)$  can be regarded as a discrete set of one-dimensional, periodic functions, which are illustrated as a set of rings in Fig. 3. Fourier transforming each of these one-dimensional functions along  $x$ , we obtain the reciprocal-space representation of the wave function,  $c(k_x, k_y)$ , which is a function of two discrete variables,  $k_x = mG_x$ , and  $k_y = nG_y$ .

### 3.2. Fourier transform of wave functions at $B \neq 0$

When a non-zero, uniform magnetic field is present,  $u(x, y)$  satisfies MPBC as in Eqs. (19)–(21),

$$u(x - a, y) = \exp \left[ i \frac{eBa}{\hbar} y \right] u(x, y), \tag{30}$$

$$u(x, y - b) = u(x, y). \tag{31}$$

Because  $u(x, y)$  is periodic in  $y$ , we can Fourier transform it along  $y$  and bring it to intermediate space,  $f(x, k_y)$ .

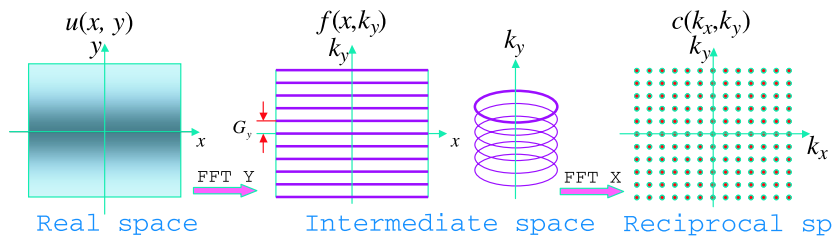


Fig. 3. At  $B = 0$ ,  $u(x, y)$  satisfies PBC. Fourier transform  $u(x, y)$  along  $y$  axis gives  $f(x, k_y)$ . Fourier transform  $f(x, k_y)$  along  $x$  axis gives  $c(k_x, k_y)$ .

$$u(x, y) = \sum_{k_y} f(x, k_y) \exp[ik_y y], \tag{32}$$

$$f(x, k_y) = \frac{1}{b} \int_{-b/2}^{b/2} u(x, y) \exp[-ik_y y] dy. \tag{33}$$

Correspondingly, use of Eq. (30) yields:

$$f(x - a, k_y) = f\left(x, k_y - \frac{eBa}{\hbar}\right). \tag{34}$$

Because  $k_y$  has to be an integer multiple of  $G_y$ , so is  $eBa/\hbar$ . This limits the magnitude of the magnetic field that can be applied to the supercell,

$$\frac{eBa}{\hbar} = n_0 G_y = n_0 \frac{2\pi}{b}, \tag{35}$$

where  $n_0$  is an arbitrary integer. As a result, the total magnetic flux through the supercell is,

$$\Phi \equiv Bab = n_0(h/e) = n_0 \Phi_0, \tag{36}$$

where  $\Phi_0 \equiv h/e$  is the fundamental quanta of magnetic flux. Therefore, the smallest magnitude of the magnetic field that can be applied to an  $a \times b$  supercell is

$$B_0 \equiv \frac{h}{eab}. \tag{37}$$

The magnetic field must be an integer multiple of  $B_0$ ,  $B = n_0 B_0$ . This constraint on  $B$  can also be directly obtained in real space. Imagine moving a point  $(x, y)$  along the border of the supercell in a complete loop,  $(x, y) \rightarrow (x + a, y) \rightarrow (x + a, y + b) \rightarrow (x, y + b) \rightarrow (x, y)$ , as shown in Fig. 1. MPBC (Eqs. (30) and (31)) requires that at the end of the loop, the wave function pick up a phase, i.e.,

$$u(x, y) \Rightarrow u(x, y) \exp\left[i \frac{eBab}{\hbar}\right]. \tag{38}$$

For consistency, the end result must be identical to  $u(x, y)$ , thus

$$\frac{eBab}{\hbar} = 2n_0\pi \tag{39}$$

which is identical to Eq. (35). Different combinations of  $\{a, b, n_0\}$  can be used to apply the same magnitude of the magnetic field. For simplicity, we focus on the case of  $n_0 = 1$  in the following discussions and leave the case of  $n_0 > 1$  to Appendix A. When  $B = B_0$ , MPBC (Eq. (34)) becomes

$$f(x - a, k_y) = f(x, k_y - G_y). \tag{40}$$

Therefore, in intermediate space, a one-dimensional function  $f(x, k_y)$  for a given value of  $k_y$  is no longer periodic in  $x$ . Instead, as  $x$  varies from the left side to the right side of the supercell, the function should be continued with a neighboring value of  $k_y$ . In other words, the set of one-dimensional functions in intermediate space forms a long spiral, as shown in Fig. 4. This topology is analogous to a screw dislocation in a crystal lattice [12].

To complete the analogy of the spiral, we define a new variable (along the spiral)

$$\hat{x} \equiv x + ak_y/G_y \tag{41}$$

and declare that in intermediate space the wave function is only a function of  $\hat{x}$ , i.e.,

$$f(\hat{x}) \equiv f(x, k_y) = f(x + a, k_y - G_y). \tag{42}$$

These definitions ensure that MPBC Eq. (40) is automatically satisfied. Therefore, the two-dimensional wave function  $u(x, y)$  becomes a one-dimensional function  $f(\hat{x})$ . The dimension reduction of wave functions by the magnetic field was noticed previously [13].

The intermediate-space wave function  $f(\hat{x})$  can be Fourier transformed along  $\hat{x}$ , resulting in the reciprocal-space representation  $c(k_{\hat{x}})$ . In principle,  $\hat{x}$  ranges from  $-\infty$  to  $\infty$ . Therefore,  $k_{\hat{x}}$  is a continuous variable

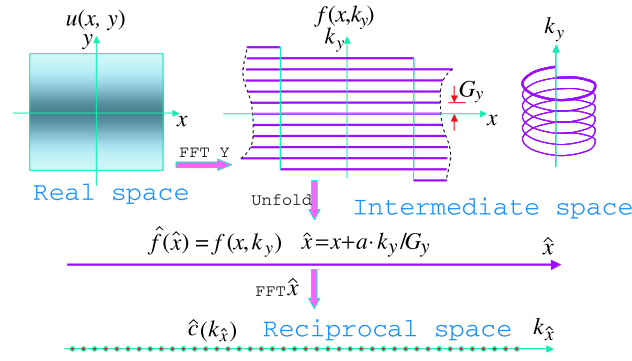


Fig. 4. At  $B = B_0$ ,  $u(x, y)$  satisfies MPBC, Eqs. (30) and (31). Fourier transform  $u(x, y)$  along  $y$  axis gives  $f(x, k_y) = \hat{f}(\hat{x})$ , where  $\hat{x} = x + ak_y/G_y$ . Fourier transform  $\hat{f}(\hat{x})$  along  $\hat{x}$  gives  $c(k_{\hat{x}})$ .

$$f(\hat{x}) = \int_{-\infty}^{\infty} c(k_{\hat{x}}) \exp[ik_{\hat{x}}\hat{x}] dk_{\hat{x}}, \quad (43)$$

$$c(k_{\hat{x}}) = \frac{1}{2\pi} \int_{-\infty}^{\infty} f(\hat{x}) \exp[-ik_{\hat{x}}\hat{x}] d\hat{x}. \quad (44)$$

In practice, the sum over  $k_y$  in Eq. (32) is truncated, e.g.  $k_y = -(N_y/2)G_y, \dots, (N_y/2 - 1)G_y$  ( $N_y$  is an even integer). Then the range of  $\hat{x}$  becomes  $[-N_y a/2, N_y a/2]$ . Hence  $k_{\hat{x}}$  becomes discretized,  $k_{\hat{x}} = n_{\hat{x}} G_{\hat{x}}$ ,  $G_{\hat{x}} = 2\pi/(N_y a)$ ,  $n_{\hat{x}}$  is an integer. The Fourier transform between  $f(\hat{x})$  and  $c(k_{\hat{x}})$  becomes

$$f(\hat{x}) = \sum_{k_{\hat{x}}} c(k_{\hat{x}}) \exp[ik_{\hat{x}}\hat{x}], \quad (45)$$

$$c(k_{\hat{x}}) = \frac{1}{N_y a} \int_{-N_y a/2}^{N_y a/2} f(\hat{x}) \exp[-ik_{\hat{x}}\hat{x}] d\hat{x}. \quad (46)$$

Combining Eqs. (32) and (45),  $u(x, y)$  can be expressed in terms of  $c(k_{\hat{x}})$  as

$$u(x, y) = \sum_{k_{\hat{x}} k_y} c(k_{\hat{x}}) \exp[ik_{\hat{x}}(x + ak_y/G_y) + ik_y y]. \quad (47)$$

In other words,  $u(x, y)$  is expanded as a sum of plane-wave-like functions, each one satisfying MPBC, and  $c(k_{\hat{x}})$  is the expansion coefficient.

### 3.3. Evaluation of $\hat{H}\psi(x, y)$ at $B \neq 0$

As mentioned before, the key step in an *ab initio* calculation is to evaluate  $\hat{H}\psi(x, y)$ , given an arbitrary trial wave function  $\psi(x, y)$ . For simplicity, consider the case of  $\kappa = 0$ , hence  $\psi(x, y) = u(x, y)$  and let  $B = B_0$ , i.e. we consider the smallest non-zero magnetic field allowed in the supercell. In this case, the Hamiltonian can be separated into three parts

$$\hat{H} = \hat{T}_x + \hat{T}_y + \hat{V}, \quad (48)$$

$$\hat{T}_x = -\frac{\hbar^2 \partial_x^2}{2m}, \quad (49)$$

$$\hat{T}_y = \frac{(-i\hbar \partial_y + eBx)^2}{2m} = \frac{\hbar^2 G_y^2}{2ma^2} \left( x - i\frac{a}{G_y} \partial_y \right)^2, \quad (50)$$

$$\hat{V} = V(x, y). \quad (51)$$

$\hat{T}_x$  is the  $x$ -component of the kinetic energy,  $\hat{T}_y$  is the  $y$ -component of the kinetic energy, and  $\hat{V}$  is the potential energy.  $\hat{T}_x$ ,  $\hat{T}_y$  and  $\hat{V}$  can be easily evaluated in reciprocal, intermediate and real spaces, respectively.  $\hat{T}_x$  simply amounts to a multiplication operator in reciprocal space,

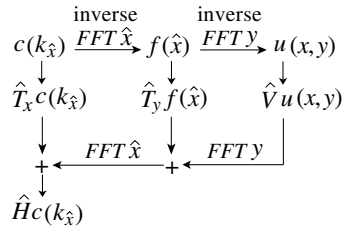


Fig. 5. Flow chart for computing  $\hat{H}c(k_{\hat{x}})$  given an arbitrary trial wave function  $c(k_{\hat{x}})$  (represented in reciprocal space). The three parts are assembled together by fast Fourier transform (FFT).

$$\hat{T}_x c(k_{\hat{x}}) = \frac{\hbar^2 k_{\hat{x}}^2}{2m} c(k_{\hat{x}}), \tag{52}$$

$\hat{T}_y$  is simply a multiplication in intermediate space,

$$\hat{T}_y f(\hat{x}) = \frac{\hbar^2 G_y^2 \hat{x}^2}{2ma^2} f(\hat{x}). \tag{53}$$

As usual,  $\hat{V}$  is simply a multiplication in real space,

$$\hat{V}u(x, y) = V(x, y)u(x, y). \tag{54}$$

Therefore, the three parts of  $\hat{H}u(x, y)$  can be evaluated separately in the three spaces and then assembled together by FFT, as illustrated in Fig. 5.

In summary, we have developed a method for computing the eigen-function of the Hamiltonian under a uniform magnetic field. The electron wave function satisfies MPBC, while the electron density (together with all other measurable field quantities) satisfies PBC. The wave function can be expressed as a sum of plane-wave-like functions, each one satisfying MPBC. The Hamiltonian can be evaluated conveniently by computing its three parts in three (real, intermediate and reciprocal) spaces and by assembling them together by FFT.

This approach was first described in [8]. It has been applied to several problems and its correctness was assessed by comparing our results with previous findings obtained using different methods. These include an electron in a quantum well, two electrons in a quantum well [14] (configuration integration), and a Hydrogen molecule [15] (Hartree–Fock). In all cases, the numerical results of this method agree well with previous results. In addition the method was applied to the study of dense, hot deuterium [16]. However, the original version of our formulation was limited to rectangular supercells and the case of  $\kappa = 0$  ( $\Gamma$ -point) only. In the following, we describe the generalization of this approach to arbitrarily tilted supercells and the case of  $\kappa \neq 0$ .

#### 4. MPBC in tilted supercell with $\kappa \neq 0$

##### 4.1. Coordinate transformation

Consider a supercell whose repeat vectors  $\mathbf{c}_1, \mathbf{c}_2, \mathbf{c}_3$  are no longer orthogonal to each other, but let the magnetic field  $\mathbf{B}$  be still parallel to  $\mathbf{c}_3$ , as shown in Fig. 6. To facilitate the discussion, we introduce two coordinate systems. The first coordinate system is formed by unit vectors  $\mathbf{e}_x, \mathbf{e}_y, \mathbf{e}_z$ , which are orthogonal to each other. The second coordinate system is formed by unit vectors  $\mathbf{e}_X, \mathbf{e}_Y, \mathbf{e}_Z$ , which are not orthogonal to each other. They are parallel to the supercell repeat vectors,

$$\mathbf{c}_1 = L_X \mathbf{e}_X, \tag{55}$$

$$\mathbf{c}_2 = L_Y \mathbf{e}_Y, \tag{56}$$

$$\mathbf{c}_3 = L_Z \mathbf{e}_Z. \tag{57}$$

As shown in Fig. 6, these two sets of unit vectors are related to each other by

$$(\mathbf{e}_X \ \mathbf{e}_Y \ \mathbf{e}_Z) = (\mathbf{e}_x \ \mathbf{e}_y \ \mathbf{e}_z)M, \tag{58}$$

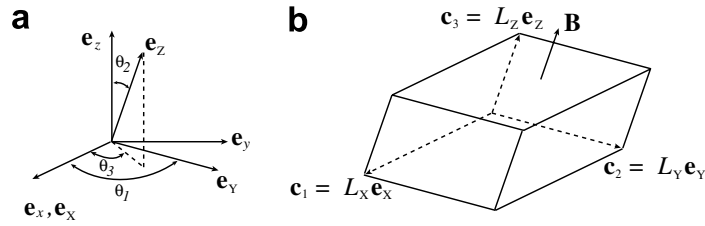


Fig. 6. (a)  $\mathbf{e}_x, \mathbf{e}_y, \mathbf{e}_z$  are unit vectors forming an orthogonal coordinate system, whereas  $\mathbf{e}_x, \mathbf{e}_y, \mathbf{e}_z$  are unit vectors that are not orthogonal to each other.  $\theta_1$  is the angle between  $\mathbf{e}_x$  and  $\mathbf{e}_y$ ;  $\theta_2$  is the angle between  $\mathbf{e}_z$  and  $\mathbf{e}_z$ ; and  $\theta_3$  is the angle between  $\mathbf{e}_x$  and the projection of  $\mathbf{e}_z$  on the  $\mathbf{e}_x$ - $\mathbf{e}_y$  plane. (b) A tilted simulation cell with repeat vectors  $\mathbf{c}_1 = L_x \mathbf{e}_x$ ,  $\mathbf{c}_2 = L_y \mathbf{e}_y$ ,  $\mathbf{c}_3 = L_z \mathbf{e}_z$ . The magnetic field  $\mathbf{B}$  is parallel to  $\mathbf{c}_3$ .

where

$$M \equiv \begin{bmatrix} 1 & \cos \theta_1 & \sin \theta_2 \cos \theta_3 \\ 0 & \sin \theta_1 & \sin \theta_2 \sin \theta_3 \\ 0 & 0 & \cos \theta_2 \end{bmatrix}. \quad (59)$$

Consider an arbitrary point  $\mathbf{x}$ , whose coordinates are  $(x, y, z)$  and  $(X, Y, Z)$  in these two coordinate systems, respectively, i.e.,

$$\mathbf{x} = (\mathbf{e}_x \ \mathbf{e}_y \ \mathbf{e}_z) \cdot \begin{bmatrix} x \\ y \\ z \end{bmatrix} = (\mathbf{e}_X \ \mathbf{e}_Y \ \mathbf{e}_Z) \cdot \begin{bmatrix} X \\ Y \\ Z \end{bmatrix}$$

Define  $T$  as the inverse of matrix  $M$ ,

$$T \equiv M^{-1} = \begin{bmatrix} 1 & -\frac{\cos \theta_1}{\sin \theta_1} & \frac{\sin \theta_2 \sin \theta_3 \cos \theta_1}{\cos \theta_2 \sin \theta_1} - \frac{\sin \theta_2 \cos \theta_3}{\cos \theta_2} \\ 0 & \frac{1}{\sin \theta_1} & -\frac{\sin \theta_2 \sin \theta_3}{\cos \theta_2 \sin \theta_1} \\ 0 & 0 & \frac{1}{\cos \theta_2} \end{bmatrix},$$

then

$$\begin{bmatrix} X \\ Y \\ Z \end{bmatrix} = T \begin{bmatrix} x \\ y \\ z \end{bmatrix}. \quad (60)$$

The chain rules of differentiation, e.g.  $\frac{\partial}{\partial x} = \frac{\partial \partial X}{\partial X \partial x} + \frac{\partial \partial Y}{\partial Y \partial x} + \frac{\partial \partial Z}{\partial Z \partial x}$ , can be summarized as,

$$\left( \frac{\partial}{\partial x} \ \frac{\partial}{\partial y} \ \frac{\partial}{\partial z} \right) = \left( \frac{\partial}{\partial X} \ \frac{\partial}{\partial Y} \ \frac{\partial}{\partial Z} \right) T. \quad (61)$$

This leads to the transformation rule in reciprocal space

$$(k_x \ k_y \ k_z) = (k_X \ k_Y \ k_Z) T. \quad (62)$$

We assume that the potential function  $V(\mathbf{x})$  is periodic in  $\mathbf{c}_1, \mathbf{c}_2$  and  $\mathbf{c}_3$ . This means that  $V$  is a periodic function of  $X, Y$ , and  $Z$ ,

$$V(X, Y, Z) = V(X - L_X, Y, Z) = V(X, Y - L_Y, Z) = V(X, Y, Z - L_Z). \quad (63)$$

Therefore, it is convenient to express the wave function as  $u(X, Y, Z)$  and discuss MPBC in terms of  $X, Y$ , and  $Z$ .

#### 4.2. Gauge choice and MPBC in tilted supercells

A constant magnetic field  $\mathbf{B} = B \mathbf{e}_z$  can be described by an infinite number of vector potentials  $\mathbf{A}(\mathbf{x})$ , corresponding to different gauge choices. We would like to choose a specific gauge that makes the expression

of MPBC as simple as possible. Similar to the choice made for orthogonal supercells (Section 2.3), let  $\mathbf{A}$  be a linear function of  $X$  and be independent of  $Y$  and  $Z$ , i.e.,

$$\mathbf{A} = BX\mathbf{a}, \tag{64}$$

where  $\mathbf{a}$  is a constant vector. It turns out that

$$\mathbf{a} = \mathbf{e}_Z \times \mathbf{e}_X = M_{33}\mathbf{e}_Y - M_{23}\mathbf{e}_Z \tag{65}$$

is the correct choice that gives rise to  $\nabla \times \mathbf{A} = B\mathbf{e}_Z$ . Therefore,

$$\mathbf{A}(\mathbf{c}_1) \cdot \mathbf{x} = BL_X\mathbf{a} \cdot \mathbf{x} = BL_X \cos \theta_2 \sin \theta_1 Y, \tag{66}$$

$$\mathbf{A}(\mathbf{c}_2) \cdot \mathbf{x} = 0, \tag{67}$$

$$\mathbf{A}(\mathbf{c}_3) \cdot \mathbf{x} = 0. \tag{68}$$

The application of MPBC (Eq. (16)) gives:

$$\begin{aligned} u(X - L_X, Y, Z) &= \exp \left[ i \frac{eBL_X}{\hbar} \cos \theta_2 \sin \theta_1 Y \right] u(X, Y, Z), \\ u(X, Y - L_Y, Z) &= u(X, Y, Z), \\ u(X, Y, Z - L_Z) &= u(X, Y, Z). \end{aligned} \tag{69}$$

In other words, the Bloch wave is a periodic function of  $Y$  and  $Z$ . This is a condition very similar to the one established for orthogonal supercells. If we move from an arbitrary point  $\mathbf{x}$  as,  $\mathbf{x} \rightarrow (\mathbf{x} + \mathbf{c}_1) \rightarrow (\mathbf{x} + \mathbf{c}_1 + \mathbf{c}_2) \rightarrow (\mathbf{x} + \mathbf{c}_2) \rightarrow \mathbf{x}$ , and return to the original point, then the wave function will pick up a non-zero phase, i.e.,

$$u(X, Y, Z) \Rightarrow \exp \left[ i \frac{eBL_X L_Y}{\hbar} \cos \theta_2 \sin \theta_1 \right] u(X, Y, Z). \tag{70}$$

For consistency, the end result must be identical to  $u(X, Y, Z)$ , thus

$$\frac{eBL_X L_Y}{\hbar} \cos \theta_2 \sin \theta_1 = 2n_0\pi, \tag{71}$$

where  $n_0$  is an integer. Therefore,

$$\Phi = BL_X L_Y \cos \theta_2 \sin \theta_1 = n_0 \frac{\hbar}{e} \equiv n_0 \Phi_0 \tag{72}$$

which means that the total flux across the supercell is again an integer multiple of the fundamental flux quanta  $\Phi_0 \equiv \hbar/e$ . Thus the magnetic field which we can apply to the supercell is quantized,

$$B = n_0 B_0, \quad B_0 = \frac{2\pi\hbar}{eL_X L_Y \cos \theta_2 \sin \theta_1}. \tag{73}$$

In terms of  $n_0$ , MPBC can be rewritten as

$$\begin{aligned} u(X - L_X, Y, Z) &= \exp \left[ i \frac{2n_0\pi Y}{L_Y} \right] u(X, Y, Z), \\ u(X, Y - L_Y, Z) &= u(X, Y, Z), \\ u(X, Y, Z - L_Z) &= u(X, Y, Z). \end{aligned} \tag{74}$$

Because  $u(X, Y, Z)$  is periodic in both  $Y$  and  $Z$  directions, we can Fourier transform it along  $Y$  and  $Z$  directions,

$$u(X, Y, Z) = \sum_{k_Y, k_Z} f(X, k_Y, k_Z) \exp[i(k_Y Y + k_Z Z)], \tag{75}$$

$$f(X, k_Y, k_Z) = \frac{1}{L_Y L_Z} \int_{-L_Y/2}^{L_Y/2} \int_{-L_Z/2}^{L_Z/2} u(X, Y, Z) \exp[-i(k_Y Y + k_Z Z)] dY dZ, \tag{76}$$

where  $k_Y = n_Y G_Y$ ,  $k_Z = n_Z G_Z$ ,  $G_Y = 2\pi/L_Y$ ,  $G_Z = 2\pi/L_Z$ ,  $n_Y$  and  $n_Z$  are integers.  $f(X, k_Y, k_Z)$  is the intermediate-space representation of the wave function, because  $X$  is a real-space variable and  $k_Y, k_Z$  are reciprocal-space variables. In intermediate space, MPBC becomes

$$f(X - L_X, k_Y, k_Z) = f(X, k_Y - n_0 G_Y, G_Z). \quad (77)$$

For simplicity, here we only consider the case of  $n_0 = 1$ . The case of  $n_0 > 1$  will be discussed in Appendix A. When  $n_0 = 1$ , Eq. (77) can be satisfied automatically by defining a new variable

$$\hat{X} \equiv X + \frac{L_X}{G_Y} k_Y = X + \frac{L_X L_Y}{2\pi} k_Y \quad (78)$$

and redefine the intermediate-space wave function as a function of  $\hat{X}$  and  $G_Z$ ,

$$f(\hat{X}, k_Z) \equiv f(X, k_Y, k_Z) = f(X - L_X, k_Y + G_Y, k_Z). \quad (79)$$

Suppose the summation over  $k_Y$  is truncated into the range  $-(N_Y/2)G_Y, \dots, (N_Y/2 - 1)G_Y$  ( $N_Y$  is an even number), then the value of  $\hat{X}$  is limited to the domain  $[-L_{\hat{X}}/2, L_{\hat{X}}/2]$ , where  $L_{\hat{X}} = N_Y L_X$ . We can then Fourier transform  $f$  along  $\hat{X}$ .

$$f(\hat{X}, k_Z) = \sum_{k_{\hat{X}}} c(k_{\hat{X}}, k_Z) \exp[ik_{\hat{X}} \hat{X}], \quad (80)$$

$$c(k_{\hat{X}}, k_Z) = \int_{-L_{\hat{X}}/2}^{L_{\hat{X}}/2} f(\hat{X}, k_Z) \exp[-ik_{\hat{X}} \hat{X}] d\hat{X}, \quad (81)$$

where  $k_{\hat{X}} = n_{\hat{X}} G_{\hat{X}}$ ,  $G_{\hat{X}} = 2\pi/L_{\hat{X}}$ ,  $n_{\hat{X}}$  is an integer. Combining Eqs. (75) and (80),  $u(X, Y, Z)$  can be expressed in terms of  $c(k_{\hat{X}}, k_Z)$  as

$$u(X, Y, Z) = \sum_{k_{\hat{X}}, k_Y, k_Z} c(k_{\hat{X}}, k_Z) \exp \left[ ik_{\hat{X}} \left( X + k_Y \frac{L_X}{G_Y} \right) + i(k_Y Y + k_Z Z) \right]. \quad (82)$$

In other words,  $u(X, Y, Z)$  is expanded as a sum of plane-wave-like functions, each satisfying MPBC, and  $c(k_{\hat{X}}, k_Z)$  is the expansion coefficient.

### 4.3. Evaluation of $\hat{H}\psi(\mathbf{x})$ at $B \neq 0$

We now discuss how to evaluate  $\hat{H}\psi(\mathbf{x})$  given an arbitrary trial wave function  $\psi(\mathbf{x})$ . In the general case of  $\boldsymbol{\kappa} \neq 0$ ,

$$\psi(\mathbf{x}) = e^{i\boldsymbol{\kappa} \cdot \mathbf{x}} u(\mathbf{x}), \quad (83)$$

$$\hat{H}\psi(\mathbf{x}) = e^{i\boldsymbol{\kappa} \cdot \mathbf{x}} \tilde{H}u(\mathbf{x}), \quad (84)$$

where

$$\tilde{H} = \frac{1}{2m} [\mathbf{p} + \hbar\boldsymbol{\kappa} + e\mathbf{A}(\mathbf{x})]^2 + V(\mathbf{x}). \quad (85)$$

Therefore, our task is equivalent to evaluate  $\tilde{H}u(X, Y, Z)$  given an arbitrary trial wave function  $u(X, Y, Z)$ . Similar to Section 3.3, we separate  $\tilde{H}u(X, Y, Z)$  into components that are convenient to evaluate in reciprocal, intermediate and real spaces, respectively.

As usual, the potential energy  $\hat{V}u(X, Y, Z) = V(X, Y, Z)u(X, Y, Z)$  is simply a multiplication operator in real space. The kinetic energy operator is the square of the following operator:

$$\begin{aligned} \mathbf{p} + \hbar\boldsymbol{\kappa} + e\mathbf{A} &= -i\hbar \left( \frac{\partial}{\partial X} \frac{\partial}{\partial Y} \frac{\partial}{\partial Z} \right) + \hbar(\kappa_x \kappa_y \kappa_z) + eBX(0 \ M_{33} - M_{23}) \\ &= -i\hbar \left( \frac{\partial}{\partial X} \frac{\partial}{\partial Y} \frac{\partial}{\partial Z} \right) T + \hbar(\kappa_x \kappa_y \kappa_z) T + \left( 0 \ \frac{2n_0\pi\hbar}{L_X L_Y} X \ 0 \right) T \\ &= -i\hbar \left( \frac{\partial}{\partial X} + i\kappa_X \frac{\partial}{\partial Y} + i\kappa_Y + \frac{2n_0\pi i}{L_X L_Y} X \frac{\partial}{\partial Z} + i\kappa_Z \right) T. \end{aligned}$$

If one defines a vector operator

$$\hat{\mathbf{b}} \equiv (\hat{b}_X \hat{b}_Y \hat{b}_Z) = \left( \frac{\partial}{\partial X} + i\kappa_X \quad i\kappa_Y + \frac{2n_0\pi i}{L_X L_Y} \hat{X} \quad \frac{\partial}{\partial Z} + i\kappa_Z \right),$$

then the kinetic energy operator can be expressed as

$$\hat{T} = -\frac{\hbar^2}{2m} \hat{\mathbf{b}} T T^T \hat{\mathbf{b}}^T. \tag{86}$$

Different components of  $\hat{\mathbf{b}}$  simply correspond to multiplications in different spaces.  $\hat{b}_X$  amounts to a multiplication in reciprocal space,

$$\hat{b}_X c(k_{\hat{X}}, k_Z) = i(k_{\hat{X}} + \kappa_X) c(k_{\hat{X}}, k_Z), \tag{87}$$

$\hat{b}_Y$  is a multiplication in intermediate space

$$\hat{b}_Y f(\hat{X}, k_Z) = i \left( \frac{n_0 G_Y}{L_X} \hat{X} + \kappa_Y \right) f(\hat{X}, k_Z), \tag{88}$$

$\hat{b}_Z$  is simply a multiplication in either reciprocal or intermediate space,

$$\hat{b}_Z c(k_{\hat{X}}, k_Z) = i(k_Z + \kappa_Z) c(k_{\hat{X}}, k_Z), \tag{89}$$

$$\hat{b}_Z f(\hat{X}, k_Z) = i(k_Z + \kappa_Z) f(\hat{X}, k_Z). \tag{90}$$

Therefore,  $\tilde{H}u(X, Y, Z)$  can be evaluated by computing its components in reciprocal, intermediate, and real spaces and by assembling them by FFT. A flow chart is illustrated in Fig. 7, in which Eq. (89) is used. The flow chart is more complicated than that for an orthogonal supercell, Fig. 5, because the matrix  $T$  is not diagonal.

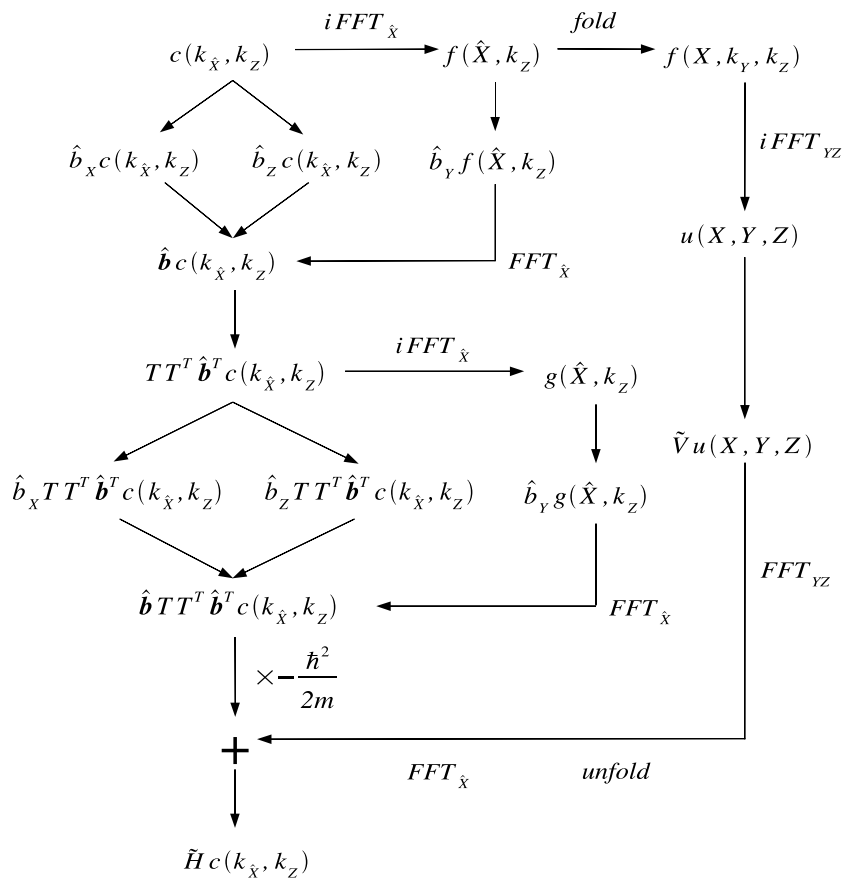


Fig. 7. Flow chart for computing  $\tilde{H}c(k_{\hat{X}}, k_Z)$  given an arbitrary trial wave function  $c(k_{\hat{X}}, k_Z)$  (represented in reciprocal space). Different components are evaluated in reciprocal, intermediate, and real spaces and assembled together by fast Fourier transform (FFT).

In our calculations, to avoid “aliasing” effects in FFT, the size of the  $c(k_x, k_z)$  array is doubled in both dimensions by padding zeros, before inverse-FFT into the intermediate space. Upon FFT back into the Fourier space, the values in the padded region usually become non-zero and are discarded. The same procedure is applied when the intermediate-space wave function is transformed into real space and back to compute the potential energy term.

## 5. Numerical results

### 5.1. Computational workload

As discussed in the previous sections, for a wave function  $\psi$  satisfying MPBC under a non-zero magnetic field, the procedure to evaluate of  $\hat{H}\psi$  is analogous to that adopted in the absence of magnetic field. Different parts of  $\hat{H}\psi$  are evaluated in different spaces and assembled together by FFT. For relatively small systems, for which the orthogonalization of electronic states (an  $\mathcal{O}(N^3)$  operation) does not dominate the scaling of the calculation, FFT is the most time consuming part of the computation, and it determines the scaling behavior of the  $\hat{H}\psi$  calculation at both zero and non-zero magnetic field. In other words, applying a non-zero magnetic field to the periodic supercell should not significantly slow down the *ab initio* calculation. The purpose of this section is to verify this statement from a numerical standpoint.

Suppose  $\psi$  is expanded as a sum of  $N_{\text{pw}}$  plane-wave basis functions (when  $B = 0$ ) or  $N_{\text{pw}}$  plane-wave-like basis functions (when  $B \neq 0$ ). The time it takes to compute  $\hat{H}\psi$  should scale in the same way as FFT, which is  $\mathcal{O}(N_{\text{pw}} \ln N_{\text{pw}})$ . In Fig. 8, we plot the wall-clock time to perform one  $\hat{H}\psi$  calculation as a function of the number of basis functions for different values of magnetic field  $B = n_0 B_0$ . The simulation cell is a cube and the basis functions are truncated in reciprocal space equally in all three directions. The calculations are performed on a Linux Pentium 4 computer with 3.0 GHz clock rate. For all cases of  $n_0 = 0, 1, 2$ , a linear relation between the computational time and  $N_{\text{pw}}$  is observed. This is because  $\ln N_{\text{pw}}$  changes very slowly over this range of  $N_{\text{pw}}$ . The computation time for  $n_0 = 1$  and  $n_0 = 2$  is almost identical to each other, and they are only about 40% higher than that of the  $n_0 = 0$  (zero magnetic field) case. This confirms that applying a finite magnetic field only brings about a moderate increase to the computational time, while the scaling behavior remains the same as the case of zero magnetic field.

### 5.2. Numerical accuracy

In this section, we study four test cases to assess the correctness and accuracy of the numerical method described above. In a previous publication [8], the validity of the method has been demonstrated for single-

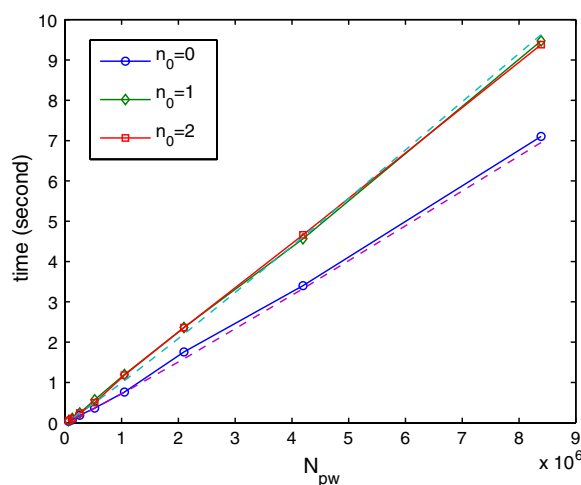


Fig. 8. Wall-clock time for one calculation of  $\hat{H}\psi$  as a function of the number basis functions. The dashed lines are numerical fits to  $C N_{\text{pw}} \ln N_{\text{pw}}$ , where the fitting parameter is  $C = 5.2 \times 10^{-8}$  (second) for  $n_0 = 0$  and  $C = 7.2 \times 10^{-8}$  (second) for  $n_0 = 1, 2$ .

electron and many-electron problems (configuration integration, Hartree–Fock, DFT), but only for the case of orthogonal supercells and  $\kappa = 0$ . Therefore, here we study the effect of the shape of the supercell, orientation of the magnetic field, and non-zero  $\kappa$ , but focus on a single electron in a quantum well.

5.2.1. *Quantum wells in arbitrarily shaped supercells*

The first test demonstrates the self-consistency of the method, by representing the same periodic array of quantum wells using different shapes of supercells. Consider an orthogonal supercell with dimension  $(10 \text{ nm})^3$ , as shown in Fig. 9a. The supercell contains a columnar quantum well, parallel to  $\mathbf{c}_3$  and with a cross section of  $4 \text{ nm} \times 4 \text{ nm}$ . Inside the quantum well the potential energy is  $V = 0$ ; outside the quantum well, the potential energy is  $V = V_0 = 600 \text{ meV}$ . The magnetic field  $\mathbf{B}$  is parallel to  $\mathbf{c}_3$  and its magnitude  $B$  is the smallest allowable value  $B_0$  ( $n_0 = 1$ ). With the orthogonal supercell, the lowest six energy levels of this quantum well array (at  $\kappa = 0$ ) can be obtained using the method described earlier [8]. They are listed on the second column of Table 1, and will be used as a benchmark for calculations using tilted supercells.

The same periodic array of quantum wells can be described by many other types of supercells, whose repeat vectors do not have to be orthogonal to each other. For example, Fig. 9b shows a supercell with repeat vectors,

$$\begin{aligned} \mathbf{c}'_1 &= \mathbf{c}_1, \\ \mathbf{c}'_2 &= \mathbf{c}_1 + \mathbf{c}_2, \\ \mathbf{c}'_3 &= \mathbf{c}_3, \end{aligned} \tag{91}$$

where  $\mathbf{c}'_1$  and  $\mathbf{c}'_2$  are not orthogonal to each other. At the same time, the physical shape of the quantum well itself remains unchanged. Because this supercell describes the same quantum well array as in Fig. 9a, it should have the same energy levels. They are listed on the third column of Table 1.

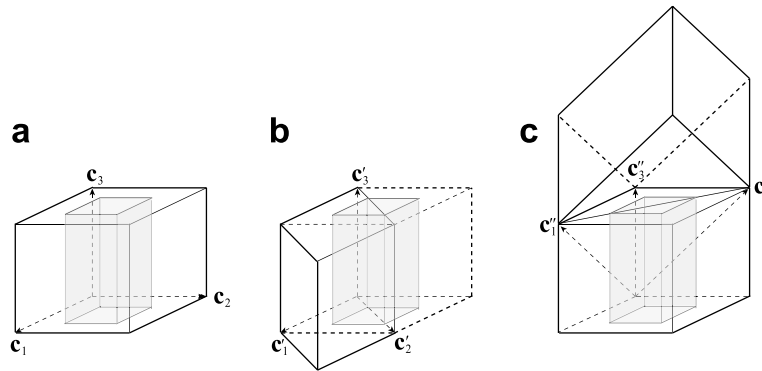


Fig. 9. Three supercells describing the same periodic quantum well array. The potential energy inside the quantum well (grey region) is zero and the potential energy outside is  $V_0 = 600 \text{ meV}$ . (a) Orthogonal supercell with repeat vectors  $\mathbf{c}_1 = L_x \mathbf{e}_x$ ,  $\mathbf{c}_2 = L_y \mathbf{e}_y$ ,  $\mathbf{c}_3 = L_z \mathbf{e}_z$ , with  $L_x = L_y = L_z = 10 \text{ nm}$ . (b) Tilted cell with repeat vectors  $\mathbf{c}'_1 = \mathbf{c}_1$ ,  $\mathbf{c}'_2 = \mathbf{c}_1 + \mathbf{c}_2$ ,  $\mathbf{c}'_3 = \mathbf{c}_3$ . This corresponds to  $L_x = L_z = 10 \text{ nm}$ ,  $L_y = 10\sqrt{2} \text{ nm}$ ,  $\theta_1 = \pi/4$ ,  $\theta_2 = 0$  and  $\theta_3 = 0$ . (c) Tilted cell with repeat vectors  $\mathbf{c}''_1 = \mathbf{c}_1 + \mathbf{c}_3$ ,  $\mathbf{c}''_2 = \mathbf{c}_2 + \mathbf{c}_3$ ,  $\mathbf{c}''_3 = \mathbf{c}_3$ . This corresponds to  $L_x = L_y = 10\sqrt{2} \text{ nm}$ ,  $L_z = 10 \text{ nm}$ ,  $\theta_1 = \pi/3$ ,  $\theta_2 = \arctan \sqrt{2}$  and  $\theta_3 = \pi/6$ .

Table 1  
The lowest six energy levels (in meV) for three different supercells shown in Fig. 9 with  $B = B_0$  ( $n_0 = 1$ )

Band no.	Model (a)	Model (b)	Model (c)
1	38.4696	38.4702	38.4698
2	53.5109	53.5114	53.5033
3	53.5109	53.5115	53.5033
4	93.5106	93.5345	93.5109
5	98.1234	98.1437	98.1239
6	98.6348	98.6353	98.6393

In Fig. 9b, the magnetic field direction ( $\mathbf{c}'_3$ ) is still orthogonal to the plane spanned by the other two repeat vectors. The method presented above is also applicable to the most general case in which  $\mathbf{c}_3$  is not orthogonal to  $\mathbf{c}_1$  or  $\mathbf{c}_2$ . Fig. 9c shows such a supercell, whose repeat vectors are

$$\begin{aligned} \mathbf{c}''_1 &= \mathbf{c}_1 + \mathbf{c}_3, \\ \mathbf{c}''_2 &= \mathbf{c}_1 + \mathbf{c}_2, \\ \mathbf{c}''_3 &= \mathbf{c}_3, \end{aligned} \tag{92}$$

in which none of the two repeat vectors are orthogonal to each other. The energy levels are listed in the last column of Table 1. The energy levels of these three different supercells all agree well with each other, confirming the correctness of the approach. In all three calculations, we use  $32 \times 32 \times 32$  plane-wave-like basis functions and use the bare mass of the electron  $m_e$ . The slight difference between the three sets of numerical results is due to the fact that different sets of basis functions are used in each calculations, since different shape of the supercell leads to different truncation schemes of basis functions in reciprocal space. This difference is further reduced if more basis functions are used in the calculations.

Because the magnetic field is  $\mathbf{B} = n_0 \mathbf{B}_0$ , we can apply the same magnetic field by specifying  $n_0 = 2$  while reducing  $B_0$  to half of the value given above. This is done by doubling the size of  $\mathbf{c}_1$ , so that the supercell now contains two quantum wells. The resulting energy levels of the three different supercells are given in Table 2. Each energy level in Table 1 now appears two times (doubly degenerate) in Table 2, because the supercell is twice as big in the latter case. Other than that, the energy values in the two tables agree well with each other, because they all describe the same array of quantum wells.

### 5.2.2. Quantum wells in a magnetic field of arbitrary direction: the case of dispersionless energy levels

In the previous section we only considered the case of a magnetic field parallel to the columnar axis of the quantum well. We now consider a magnetic field that is at an angle  $\theta = 54^\circ$  with respect to the plane of a plate-like quantum well. Again, we compute the energy level of this system using three different but equivalent supercells and compare their numerical results.

In Fig. 10a, the plane of the quantum well is parallel to two repeat vectors,  $\mathbf{c}_1$  and  $\mathbf{c}_2$ , and the magnetic field direction ( $\mathbf{c}_3$ ) is at  $\theta = 54^\circ$  with  $\mathbf{c}_1$ . In Fig. 10b, the same geometry is described using an orthogonal supercell.

Table 2  
The lowest six energy levels (in meV) for three different supercells that are twice as big as those shown in Fig. 9

Band no.	Model (a)	Model (b)	Model (c)
1	38.4665	38.4721	38.4665
2	38.4674	38.4706	38.4675
3	53.5080	53.5120	53.5064
4	53.5081	53.5127	53.5063
5	53.5091	53.5126	53.5076
6	53.5077	53.5130	53.5106

This reduces  $B_0$  by half. Together with  $n_0 = 2$ , the total magnetic field  $\mathbf{B} = n_0 \mathbf{B}_0$  is the same as before.

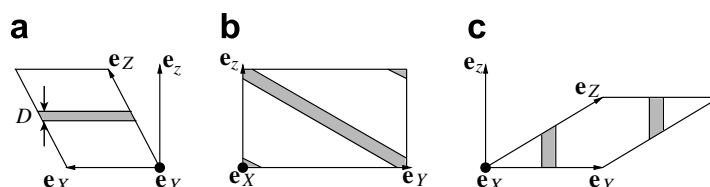


Fig. 10. A periodic array of plate-like quantum wells represented by three supercells. The potential inside the quantum well (shaded region) is zero and the potential outside is  $V_0 = 225$  meV. The width of the quantum well is  $D = 3.5674$  nm. (a) A tilted supercell with quantum well plate parallel to the  $x$ - $y$  plane.  $L_x = 14$  nm,  $L_y = 14.119$  nm,  $L_z = 37.082$  nm,  $\theta_1 = \pi/2$ ,  $\theta_2 = 36^\circ$ ,  $\theta_3 = 0$ . (b) An orthogonal supercell with the quantum well tilted with respect to all repeat vectors.  $L_x = 3.1333$  nm,  $L_y = 51.039$  nm,  $L_z = 37.082$  nm,  $\theta_1 = \pi/2$ ,  $\theta_2 = 0$ ,  $\theta_3 = 0$ . (c) A tilted supercell with the quantum well normal to the  $x$ - $y$  plane.  $L_x = 9.069$  nm,  $L_y = 30$  nm,  $L_z = 37.082$  nm,  $\theta_1 = \pi/2$ ,  $\theta_2 = 54^\circ$ ,  $\theta_3 = \pi/2$ .

Because  $\mathbf{c}_3$  and  $\mathbf{c}_2$  are orthogonal to each other, the quantum well plane is at an angle  $\theta = 54^\circ$  with  $\mathbf{c}_3$  and at an angle  $\pi/2 - \theta = 36^\circ$  with  $\mathbf{c}_2$ . In Fig. 10c, the magnetic field direction  $\mathbf{c}_3$  is at  $\pi/2 - \theta = 36^\circ$  with  $\mathbf{c}_2$  and the quantum well plane is perpendicular to  $\mathbf{c}_2$ . All three supercells correspond to the same physical problem. The width of the quantum well is 3.5674 nm and the effective mass of the electron is  $m_{\text{eff}} = 0.067m_e$ , corresponding to electrons in GaAs–Al<sub>0.3</sub>GaAs<sub>0.7</sub>. The magnitude of the magnetic field is  $B = 25.861$  T and the Bloch wave vector  $\boldsymbol{\kappa}$  is set to zero. The lowest six energy levels for these three supercells are listed in Table 3. The numerical results for these three supercells agree well with each other. However, the three supercells are not equally convenient to use. With the tilted supercell represented in Fig. 10a, we can easily vary the orientation of the magnetic field with respect to the quantum well by tilting  $\mathbf{e}_z$ , without changing other aspects of the supercell. In comparison, changing the magnetic field orientation with respect to the quantum well in Fig. 10b would be much more cumbersome; the aspect ratio of the supercell and the position of the quantum well would have to be redesigned for each magnetic field orientation. This would make it difficult to compare results from different magnetic field orientations. Also, when the magnetic field is tilted with respect to the quantum well, as is the case here, the energy levels are found to be independent of the Bloch wave vector  $\boldsymbol{\kappa}$ , consistent with previous results [17]. However, if the magnetic field is parallel to the plane of the quantum well, the energy levels are not dispersionless and this is the case presented in the next section.

### 5.2.3. Quantum wells parallel to the magnetic field: the case of dispersive energy levels

We now consider the band structure of a plate-like quantum well under a uniform magnetic field, as shown in Fig. 11a. The magnetic field direction ( $\mathbf{c}_3$ ) is parallel to the quantum well plane and the Bloch vector  $\boldsymbol{\kappa}$  is varied along the  $\kappa_x$  direction. The thickness of the quantum well is  $L \approx 3.6$  nm. The size of the supercell is  $L_x = 1.5992$  nm and  $L_y = 100$  nm. The magnitude of the magnetic field is  $B \approx 26$  T. The potential energy

Table 3  
The lowest six energy levels (in meV) for three different supercells shown in Fig. 10

Band no.	Model (a)	Model (b)	Model (c)
1	129.0465	129.0459	129.0456
2	164.9916	164.9897	164.9888
3	200.8959	200.8927	200.8917
4	236.7851	236.7809	236.7234
5	254.1594	254.1587	254.1130
6	265.9358	265.9352	265.8732

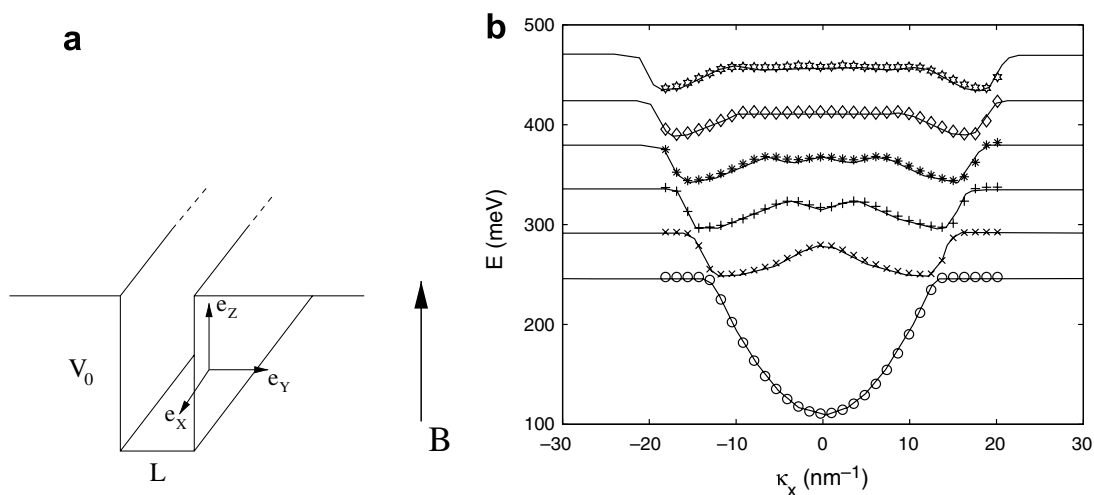


Fig. 11. (a) The energy level of a plate-like quantum well.  $V$  is only a function of  $y$  and is zero inside the well and  $V_0$  outside the well. The magnetic field is parallel to the  $z$  direction, i.e. within the plane of the quantum well. (b) Energy levels of the quantum well as a function of Bloch wave vector  $\kappa_x$ . Lines correspond to previous data [18] and symbols correspond to our results.  $\kappa_x$  is proportional to the distance between the center of the electron wave packet and the center of the quantum well.

is zero inside the quantum well and is  $V_0 = 225$  meV outside. The effective mass of the electron is  $m_{\text{eff}} = 0.067m_e$ . The same problem has been studied previously by [18]; their data will be used for comparisons here.

The band structure is plotted in Fig. 11b. As a result of our choice of gauge, the magnetic field localizes the electron wave function in the  $y$ -direction.  $\kappa_x$  corresponds to the center of the electron wave packet. When  $\kappa_x = 0$ , the electron is at the center of the quantum well. The ground state energy is the lowest in this case. At sufficiently large  $\kappa_x$ , the electron wave packet is mostly immersed in the constant-potential-energy region in which  $V = V_0$ . In this case, the energy levels should reduce to Landau levels plus a constant,  $V_0$ . As shown in Fig. 11b, our results agree well with those reported previously [18]. Notice that in the previous study, the energy levels of an isolated quantum well are computed as a function of the center of the electron packet, which did not require MPBC or a supercell. In this study, we considered a periodic array of quantum wells. The size of the supercell is large enough so that the interference between neighboring quantum wells are small. Nonetheless, if  $\kappa_x$  becomes too large, then the center of the electron wave packet will move to the neighboring quantum well. In this case, the two results will deviate from each other. While the energy levels from [18] will remain constant at large  $\kappa_x$ , our energies will be periodic functions of  $\kappa_x$ . When the separation between neighboring quantum wells is small, their interference will give rise to a non-trivial band structure. The band structure of a periodic array of quantum wells under a uniform magnetic field is presented in Section 5.3.

#### 5.2.4. Potential well in a magnetic field of arbitrary direction

We turn to the study of the effect of the orientation of the magnetic field with respect to a potential well. The potential is a quadratic function of  $z$ ,  $V(z) = Az^2$ . The iso-surfaces of this potential function are planes orthogonal to the  $\mathbf{e}_z$  direction. The magnetic field is tilted at an arbitrary angle with the  $\mathbf{e}_z$  direction. The energy levels as a function of the magnitude and orientation of the magnetic field have been obtained analytically [19] and are used as benchmarks here.

Fig. 12 plots the separation between neighboring energy levels as a function of magnetic field strength, both in unit of  $\hbar\omega_0$ ,  $w_0 = \sqrt{2A/m^*}$ , when the magnetic field is at  $0^\circ$ ,  $30^\circ$ ,  $60^\circ$  and  $90^\circ$  with the  $\mathbf{e}_z$  direction. The agreement between our numerical results and previous analytic results is excellent.

### 5.3. Magnetic band structure

In this section, we present calculations of a magnetic band structure to illustrate the benefit of our method over existing, alternative approaches. Magnetic band structures have been computed before, using tight binding models [20], effective Hamiltonians [21], or grid discretized Hamiltonians [22], but not at the *ab initio* level

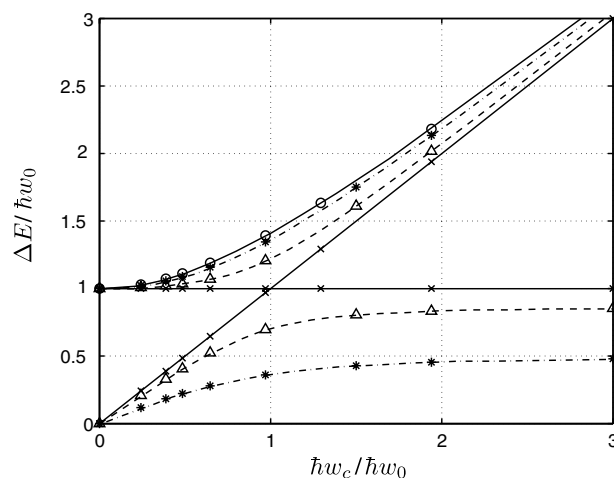


Fig. 12. Energy gap of a parabolic potential well  $V(z)$  for different angle  $\theta$  between the magnetic field and  $z$ -axis. Lines are previous data and symbols are our result. The top continuous line is for  $\theta = 90^\circ$ . Dashed dot lines are for  $\theta = 60^\circ$  and dashed lines are for  $\theta = 30^\circ$ . Two straight solid lines are for  $\theta = 0^\circ$ .

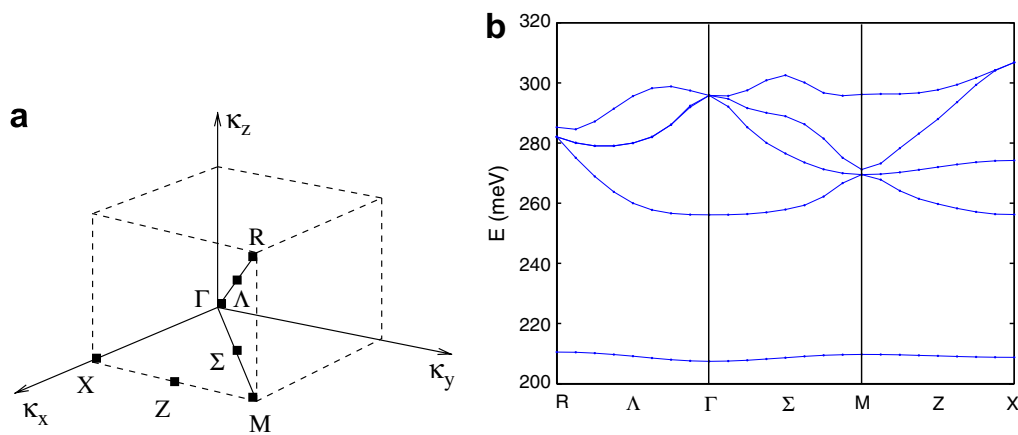


Fig. 13. (a) First Brillouin Zone and high symmetry points of sc structure. (b) Electronic band structure (without magnetic fields).

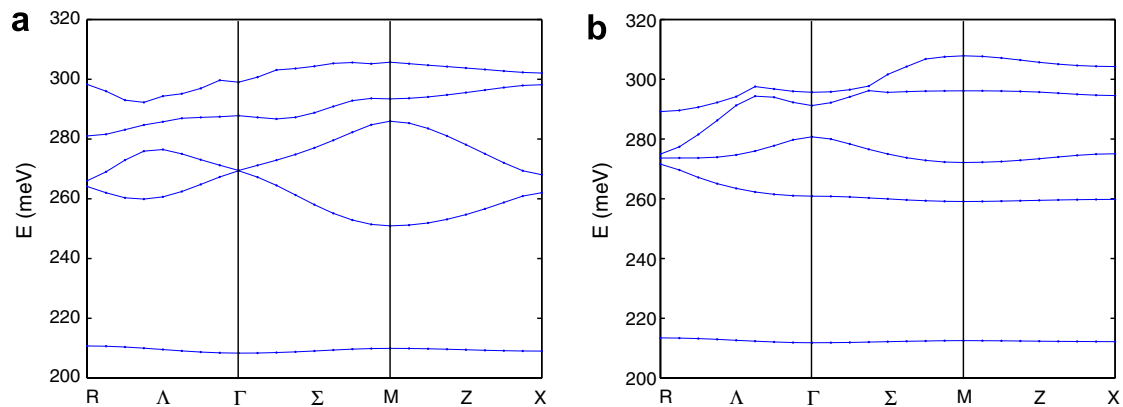


Fig. 14. Magnetic band structures of a periodic array of quantum dots forming an sc lattice: (a)  $B = 10.34$  T, (b)  $B = 20.68$  T.

in which the electron wave functions are expressed as smooth functions in real space and expanded in terms of plane waves. Here we present the first *ab initio* calculation of a magnetic band structure. In particular, we computed the band structure of a simple cubic superlattice with and without magnetic field. The size of the supercell is  $L_X = 20$  nm,  $L_Y = 20$  nm,  $L_Z = 20$  nm and the axes are orthogonal. We assume that our sc lattice is composed of quantum dots and the potential of each quantum dot is modeled by a cubic, finite quantum well of size is  $5$  nm  $\times$   $5$  nm  $\times$   $5$  nm; the potential energy is zero inside the quantum dot and  $243$  meV outside. The effective electron mass is set to  $m_{\text{eff}} = 0.067m_e$ . The first Brillouin zone and the band structure in the absence of a magnetic field are shown in Fig. 13, which is in good agreement with the results of Li et al. [23], who also used a plane wave basis to calculate the electronic band structure of the same model system.

Next, we applied a uniform magnetic field in the  $e_z$  direction. The strength of the magnetic field is quantized by Eq. (73), i.e.  $B = n_0 B_0$ . The results for  $B = B_0$  and  $B = 2B_0$  are given in Fig. 14, where  $B_0 = 10.34$  T. A comparison between the band structures obtained with  $B = 0$ ,  $B = 10.34$  T and  $B = 20.68$  T shows that the presence of a magnetic field introduces a weak change on the ground state of the systems, while the changes in the excited states are substantial. It is also interesting to note that the energy band gap decreases at  $B = 10.34$  T and increases at  $B = 20.68$  T, compared with  $B = 0$  case.

## 6. Summary and outlook

We have presented a method to introduce a constant magnetic field in solving the Schrödinger's equation for electrons, within an *ab initio* formulation. The method retains the numerical advantages of supercell approaches with PBC, plane-wave-like basis, and fast Fourier transforms, and it is applicable to arbitrarily

tilted supercell and non-zero  $\mathbf{k}$ -points. This is a first step towards enabling *ab initio* molecular dynamics of condensed matter under a magnetic field. The next step towards a working scheme for *ab initio* MD simulations involves computing forces on the nuclei. The presence of an external magnetic field requires the calculation of Berry's phase of the electronic wavefunctions, which produces an effective Lorentz force acting onto the nuclei [24], in addition to the usual electrostatic or Hellman–Feynman force from derivatives of the Kohn–Sham energy. The calculation of forces on ions will be dealt with in a forthcoming paper. Other open problems include how to account for spin–orbit coupling, and whether or not the exchange and correlation potential entering the functional used to solve Kohn–Sham equations needs to be revised when a strong magnetic field is present.

### Acknowledgments

This work is partly supported by the DOE/SciDAC project on Quantum Simulation of Materials and Nanostructures. Eunseok Lee gratefully acknowledges support from the Samsung Scholarship (formerly the Samsung LeeGunHee Scholarship Foundation).

### Appendix A. MPBC at $n_0 > 1$

It would be convenient if we can vary the strength of the magnetic field,  $B = n_0 B_0$ , by changing the value of  $n_0$ , while keeping the supercell shape unchanged. When  $n_0 > 1$ , the implementation of MPBC is slightly more complicated than the case of  $n_0 = 1$ . For simplicity, we only discuss the case of orthogonal cell and zero  $\mathbf{k}$ -point in this appendix. First of all, when  $n_0 > 1$ , MPBC in intermediate space becomes

$$f(x - a, k_y) = f(x, k_y - n_0 G_y). \quad (93)$$

This means that as  $x$  moves from the left side to the right side of the supercell, the function  $f(x, k_y)$  should continue with  $k_y$  shifted by  $n_0 G_y$ , as shown in Fig. 15. Therefore, the function  $f(x, k_y)$  can be considered as

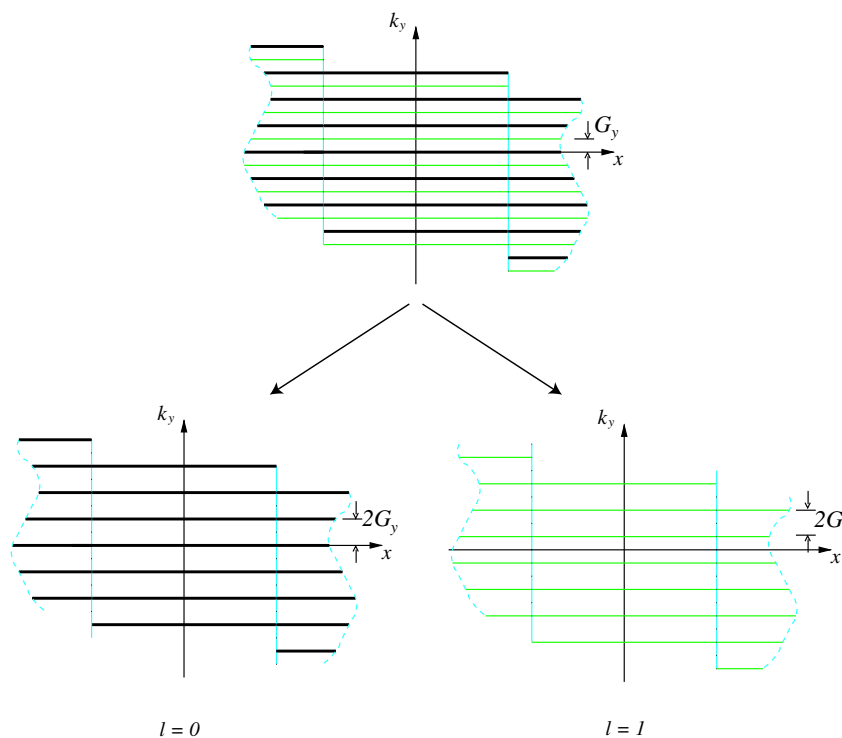


Fig. 15. MPBC in intermediate space for  $n_0 = 2$ ,  $B = 2B_0$ . Wave function  $f(x, k_y)$  can be rearranged into  $f(\hat{x}, l)$ , where  $l = 0, 1$ .

$n_0$  spirals interlaced together. Notice that it is no longer correct to declare  $f(x, k_y) = f(\hat{x})$ , where  $\hat{x} \equiv x + \frac{ak_y}{n_0G_y}$ , because such a definition would imply,

$$f(x - a/n_0, k_y) = f(x, k_y - G_y) \tag{94}$$

which is not true.

Instead, we need to introduce new variables in intermediate space. Let

$$k_y/G_y = qn_0 + l, \tag{95}$$

where  $q$  and  $l$  are integers ( $0 \leq l < n_0$ ).  $q$  and  $l$  are the quotient and residue when  $k_y/G_y$  is divided by  $n_0$ . The proper definition of  $\hat{x}$  is,

$$\hat{x} \equiv x + \frac{a}{n_0} \left( \frac{k_y}{G_y} - l \right) = x + aq. \tag{96}$$

The intermediate-space wave function can be re-written as

$$f(x, k_y) = f(\hat{x}, l), \tag{97}$$

where  $l = 0, 1, \dots, n_0 - 1$ . When  $n_0 = 1$ ,  $l$  can only be zero, and the intermediate-space wave function reduces to a one-dimensional function  $f(\hat{x})$ . Suppose the sum over  $k_y$  is truncated, e.g.  $k_y = -(N_y/2)G_y, \dots, (N_y/2 - 1)G_y$  (assuming that  $N_y$  is an integer multiple of  $2n_0$ ). Then the range of  $\hat{x}$  becomes  $[-N_y a / (2n_0), N_y a / (2n_0)]$ .

Fourier transforming  $f(\hat{x}, l)$  along  $\hat{x}$  for each  $l$  leads to the reciprocal-space wave function,

$$f(\hat{x}, l) = \sum_{k_{\hat{x}}} c(k_{\hat{x}}, l) \exp[ik_{\hat{x}}\hat{x}], \tag{98}$$

$$c(k_{\hat{x}}, l) = \frac{n_0}{N_y a} \int_{-N_y a / (2n_0)}^{N_y a / (2n_0)} f(\hat{x}, l) \exp[-ik_{\hat{x}}\hat{x}] d\hat{x}. \tag{99}$$

Combining Eqs. (32) and (98),  $u(x, y)$  can be expressed in terms of  $c(k_{\hat{x}}, l)$  as,

$$u(x, y) = \sum_{k_{\hat{x}}k_y} c(k_{\hat{x}}, l) \exp[ik_{\hat{x}}(x + aq) + ik_y y], \tag{100}$$

where  $k_y/G_y = qn_0 + l$ . In other words,  $u(x, y)$  is expanded as a sum of plane-wave-like functions, each one satisfying MPBC, and  $c(k_{\hat{x}}, l)$  is the expansion coefficient.

To evaluate  $\hat{H}\psi(x, y)$  given an arbitrary trial wave function  $\psi(x, y)$ , we separate  $\hat{H}$  into three parts, similar to the case of  $n_0 = 1$  (Section 3.3),

$$\hat{H} = \hat{T}_x + \hat{T}_y + \hat{V}, \tag{101}$$

$$\hat{T}_x = -\frac{\hbar^2 \partial_x^2}{2m}, \tag{102}$$

$$\hat{T}_y = \frac{(-i\hbar \partial_y + eBx)^2}{2m} = \frac{n_0^2 \hbar^2 G_y^2}{2ma^2} \left( x - i \frac{a}{n_0 G_y} \partial_y \right)^2, \tag{103}$$

$$\hat{V} = V(x, y). \tag{104}$$

$\hat{T}_x$  is the  $x$ -component of the kinetic energy,  $\hat{T}_y$  is the  $y$ -component of the kinetic energy, and  $\hat{V}$  is the potential energy.  $\hat{T}_x$ ,  $\hat{T}_y$ , and  $\hat{V}$  can be easily evaluated in reciprocal, intermediate and real spaces, respectively.  $\hat{T}_x$  is simply a multiplication in reciprocal space,

$$\hat{T}_x c(k_{\hat{x}}, l) = \frac{\hbar^2 k_{\hat{x}}^2}{2m} c(k_{\hat{x}}, l), \tag{105}$$

$\hat{T}_y$  is simply a multiplication in intermediate space,

$$\hat{T}_y f(\hat{x}, l) = \frac{n_0^2 \hbar^2 G_y^2}{2ma^2} \left( \hat{x} + \frac{al}{n_0} \right)^2 f(\hat{x}, l). \tag{106}$$

As before,  $\hat{V}$  is simply a multiplication in real space,

$$\hat{V}u(x, y) = V(x, y)u(x, y). \quad (107)$$

Therefore, the three parts of  $\hat{H}u(x, y)$  can be evaluated separately in the three spaces and then assembled together by FFT, similar to that illustrated in Fig. 5. The same procedure can be generalized to arbitrarily tilted supercells and non-zero  $\mathbf{k}$ -points. The details are omitted here to save space. This procedure is implemented in our code and is used in test case 4 (Section 5.2.4) where the magnitude of the magnetic field is changed by varying  $n_0$  for a fixed supercell.

## References

- [1] R.M. Martin, *Electronic Structure: Basic Theory and Practical Methods*, Cambridge University Press, Cambridge, 2003.
- [2] R. Car, M. Parrinello, *Phys. Rev. Lett.* 55 (1985) 2471.
- [3] P. Pulay, in: K.P. Lawley (Ed.), *Ab Initio Methods in Quantum Chemistry II*, Wiley, Chichester, 1987, p. 241.
- [4] S. Baroni, P. Giannozzi, A. Testa, *Phys. Rev. Lett.* 58 (1987) 1861;  
F. Mauri, S.G. Louie, *Phys. Rev. Lett.* 76 (1996) 4246;  
F. Mauri, B. Pfroemmer, S.G. Louie, *Phys. Rev. Lett.* 77 (1996) 5300.
- [5] H. Ruder, G. Wunner, H. Herold, F. Geyer, *Atoms in Strong Magnetic Fields*, Springer, Berlin, 1994.
- [6] I. Souza, J. Iniguez, D. Vanderbilt, *Phys. Rev. Lett.* 89 (2002) 117602;  
P. Umari, A. Pasquarello, *Phys. Rev. Lett.* 89 (2002) 157602.
- [7] A. Trellakis, *Phys. Rev. Lett.* 91 (2003) 056405.
- [8] W. Cai, G. Galli, *Phys. Rev. Lett.* 92 (2004) 186402.
- [9] The Bohr–Van Leeuwen Theorem states a related behavior – that the thermal equilibrium magnetization of a collection of electrons must always vanish in classical statistical mechanics. See for example N.W. Ashcroft, N.D. Mermin, *Solid State Physics*, vol. 646, Saunders College, Philadelphia, 1976, p. 269, 646.
- [10] E. Brown, *Phys. Rev.* 133 (1964) A1038.
- [11] M.C. Payne, M.P. Teter, D.C. Allen, T.A. Arias, J.D. Joannopoulos, *Rev. Mod. Phys.* 64 (1992) 1045.
- [12] J.P. Hirth, J. Lothe, *Theory of Dislocations*, Wiley, New York, 1982.
- [13] G.M. Obermair, H.-J. Schellnhuber, *Phys. Rev. B* 23 (1981) 5185.
- [14] C.E. Creffield, J.H. Jefferson, S. Sarkar, D.L.J. Tipton, *Phys. Rev. B* 62 (2000) 7249.
- [15] T. Detmer, P. Schmelcher, F.K. Diakonov, L.S. Cederbaum, *Phys. Rev. A* 56 (1997) 1825.
- [16] G. Galli, R.Q. Hood, A.U. Hazi, F. Gygi, *Phys. Rev. B* 61 (2000) 909;  
S. Bonev, B. Militzer, G. Galli, *Phys. Rev. B* 69 (2004) 014101.
- [17] T.M. Fromhold et al., *Phys. Rev. Lett.* 75 (1995) 1142 (1989).
- [18] Y. Ergun, I. Sokmen, H. Sari, S. Elagoz, M.C. Arıkan, *Semicond. Sci. Technol.* 12 (1997) 802–807.
- [19] J.C. Mann, *Two-dimensional Systems, Heterostructures and Superlattices*, *Solid State Sciences* 53, in: G. Bauer et al. (Eds.), Springer, Berlin, 1984, p. 183.
- [20] M. Graf, *Phys. Rev. B* 51 (1995) 4940.
- [21] M. Taut, *Phys. Rev. B* 72 (2005) 165304.
- [22] M. Governale, C. Ungarelli, *Phys. Rev. B* 58 (1998) 7816.
- [23] S. Li, J. Xia, *J. Appl. Phys.* 84 (1998) 3710.
- [24] R. Resta, *J. Phys.: Condes. Matter* 12 (2000) R107.